

Pulsation of M-type Mira variables with moderately different mass: search for observable mass effects

M.J. Ireland¹, M. Scholz^{1,2}, P.G. Tuthill¹, P.R. Wood³

¹*School of Physics, University of Sydney NSW 2006, Australia*

²*Institut für Theoretische Astrophysik der Universität Heidelberg, Albert-Überle-Str.2, 69120 Heidelberg, Germany*

³*Research School for Astronomy and Astrophysics, Australian National University, Canberra ACT 2600, Australia*

2 October 2018

ABSTRACT

Models of M-type Miras with masses of $1 M_{\odot}$ and $1.2 M_{\odot}$, i.e. with envelope masses of about $0.4 M_{\odot}$ and $0.6 M_{\odot}$, have been constructed, and a comparison has been made of their observable properties. Geometric pulsation of continuum-forming layers is found to be little affected by the mass difference. The influence of molecular contamination of near-infrared continuum bandpasses upon interferometrically measured fit diameters ranges from undetectable to quite significant. Some pulsation cycles of the lower-mass model Mira show substantially stronger contamination than that found in any cycle of the higher-mass star. Observations which sample pulsation phase well and continuously are crucial for avoiding misinterpretations, because the assignment of absolute pulsation phases is inherently uncertain by at least 0.1 cycles, diameter changes may be strongly phase-dependent, and cycle-to-cycle variations may be substantial. In accord with expectations, we find that cycle-to-cycle variations that show up in light curves and in near-continuum diameters tend to be larger and more common in the low-mass models, leading to one possible way to discriminate mass. Two other methods, based on high-precision measurements of the pulsation amplitude and on derivation of pre-maximum effective temperatures from diameter measurements, are also discussed. High-layer features that may be strongly affected by mass are not well described by present dust-free models.

Key words: techniques: interferometric – stars: variables: Miras – stars: AGB and post-AGB

1 INTRODUCTION

The typical mass of an M-type Mira variable is assumed to be of the order of $1 M_{\odot}$ from general considerations of AGB evolution and pulsation theory. This value is uncertain by a few tenths of a solar mass, but no method is known for accurately determining the mass of a non-binary Mira. Wyatt & Cahn (1983) derive masses between 1.00 and $1.66 M_{\odot}$ for the progenitor main-sequence stars of 124 Miras (10 percent of these larger than $1.30 M_{\odot}$) from an analysis of their kinematic properties. The “round” value of $1.0 M_{\odot}$ is often adopted in Mira modelling. Recent model studies of the disk brightness distribution of these stars, however, seem to indicate that moderate changes of the stellar mass lead to effects on geometric pulsation (Hofmann, Scholz & Wood 1998, henceforth HSW98; Jacob & Scholz 2002, henceforth JS02) that might be accessible to properly designed observations. From the uniform-disk (UD, or other simple disk-brightness) fit radii given by HSW98 and JS02, one suspects that both the pulsation of continuum-forming layers and the molecular contamination of near-continuum bandpasses that partly masks geometric pulsation (Ireland, Scholz & Wood 2004, henceforth ISW04) may depend on mass. Since, however, the HSW98 and JS02 studies consider only two phases per cycle and centre-to-limb variation (CLV) of the disk intensity often varies strongly with phase (ISW04), a more elaborated model

set is needed for assessing mass effects. We compare in this study two series of Mira pulsation models which have identical luminosity and linear period but a moderately different mass for the parent star, and look for observable pulsation differences.

There are only a few interferometric observation of the periodic variation of the near-continuum angular diameter available in the literature: Tuthill, Haniff & Baldwin (1995), *o* Cet, $0.833 \mu\text{m}$, $0.902 \mu\text{m}$; Burns et al. (1998), R Leo, $0.833 \mu\text{m}$, $0.940 \mu\text{m}$; Perrin et al. (1999), R Leo, $2.2 \mu\text{m}$ K bandpass; Young et al. (2000), χ Cyg, S-type Mira, $0.905 \mu\text{m}$; Thompson, Creech-Eakman & Van Belle (2002), S Lac, $2.2 \mu\text{m}$ K bandpass; Woodruff et al. (2004), *o* Cet, $2.2 \mu\text{m}$ K bandpass. None of these observations covers one or more full cycles, and observed phase intervals tend to be fairly narrow. They probe a combination of continuum pulsation and phase-dependent molecular-band absorption in the observed bandpasses (ISW04).

2 MODELS

This study is based upon two series of complete self-excited models of HSW98, supplemented by additional phases given in Tej et al. (2003b, henceforth TLSW03), in ISW04 and in this paper. The parameters of these series were chosen to represent the M-type Mira

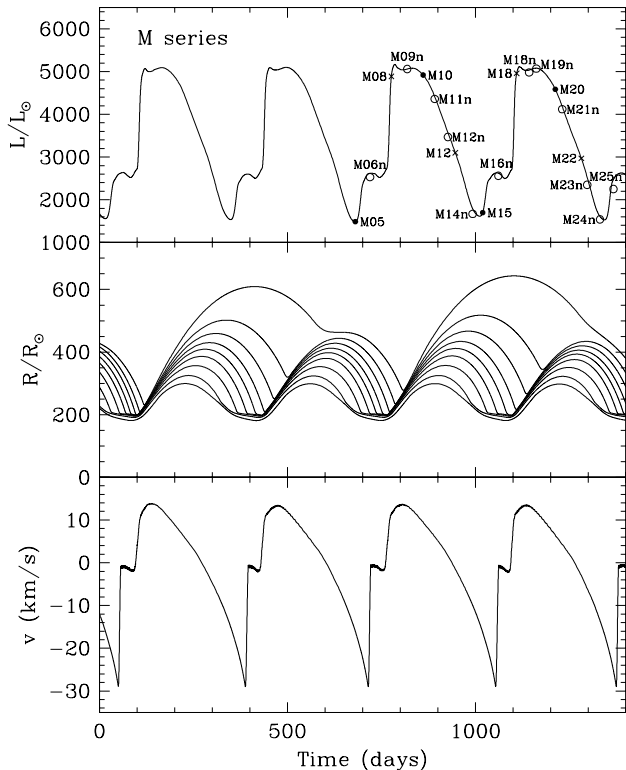


Figure 1. Luminosity (top panel), radii of selected mass zones (middle) and the velocity of the 5th mass zone from the centre (bottom) of the M model series (see HSW98). One cycle is covered by about 1400 pulsation model time-steps. Those time-steps for which a detailed non-gray atmospheric model was constructed (see HSW98) and whose properties are discussed in this study are marked by dots (models of HSW98), crosses (TLSW03) and circles (this work).

prototypes *o* Cet and R Leo. The non-pulsating parent star has solar metallicity, luminosity $L/L_{\odot}=3470$, and mass $M/M_{\odot}=1.0$ for the P model series and $M/M_{\odot}=1.2$ for the M series. The linear pulsation period is 332 days in both cases. This comparative study is aimed at seeing whether, at a given period, observable characteristics vary in a way that might be used to estimate the star’s mass. Note that the 20 percent increase in mass does, in fact, imply an increase of about 50 percent in envelope mass as the typical AGB core mass is about 0.6 solar masses. The $\tau_{\text{Ross}}=1$ Rosseland radius of the parent star is $R_p/R_{\odot}=241$ for the P series and $R_p/R_{\odot}=260$ for the M series, corresponding to an effective temperature $T_{\text{eff}} \propto (L/R^2)^{1/4}$ of 2860K (P) and 2750K (M).

In the HSW98 model series, the mixing length l enters the pulsation calculation as a free parameter that is so chosen that, for the adopted luminosity and mass, the pulsation period was close to the 332 day period of *o* Cet. It is $2.06H_p$ for the P models and $1.73H_p$ for the M models (H_p = pressure scale height). Since, however, the choice of l is only a very minor factor in overall pulsation behaviour, predicted differences between the two model series are essentially generated by the difference of mass. Details regarding

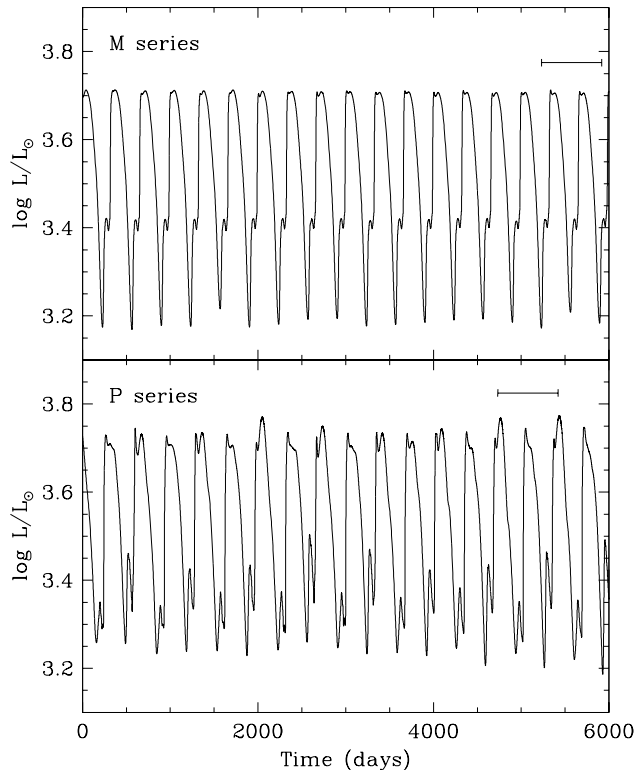


Figure 2. Luminosity for many cycles of the M model series (top panel) and P model series (lower panel). The horizontal bars indicate the range of phases used in this paper.

assumptions of modelling pulsation and the dynamic atmosphere are described in HSW98. The models of TLSW03 and ISW04 and the new models given here are constructed in the same way as the HSW98 models.

Using the LMC period-luminosity relation (e.g. Feast et al. 1989; Hughes & Wood 1990) the adopted luminosity of the model series appears to be significantly too low. However, the distances required for the model series to match the J- and K-band magnitudes of the prototype Mira stars *o* Cet and R Leo is within 2σ of their HIPPARCOS distances given by Knapp et al. (2003). The HIPPARCOS distances would seem to indicate that the adopted luminosity is slightly too high for *o* Cet and slightly too low for R Leo, resulting in an unclear answer for the best model luminosity to adopt (see the discussion in ISW04).

Since the P model series of HSW98 have cycles with strikingly different amounts of molecular contamination of near-continuum bandpasses (JS02), ISW04 selected 2 successive cycles (of 4 cycles given in HSW98) that show a very low and a very high contamination. Inspection of a large sequence of cycles of our two model series shows that cycle-to-cycle variations are still present but much less pronounced in the M series, and the 2 cycles given in HSW98 and in this paper should illustrate the typically very modest differences between cycles in a more massive Mira. Since phase assignment is only approximate for the models listed

in the HSW98/TLW03 tables, we have re-assigned more accurate phases to the full set of HSW98/TLW03 models and our new set of supplementary models in order to study detailed phase effects. The visual phases which are used to identify the models of the series are approximate and precede bolometric phases by 0.1 (Lockwood & Wing 1971; cf. HSW98). Note, however, that the absolute zero point of any phase assignment is uncertain by at least 0.05 to 0.1 due to the irregularities of modelled (HSW98) and observed (e.g. Whitelock, Marang & Feast 2000) Mira light curves. Furthermore, the actual pulsation period that arises after pulsation sets in differs slightly from the linear pulsation period of the parent star. It is about 317 days for the P model series and about 341 days for the M series. Individual cycle lengths may readily vary by a few days. Altogether, absolute phases in Table 1 are uncertain by at least 0.1 whereas relative phases are accurate to about 0.01 to 0.02.

Figure 1 is the equivalent of Figure 2 of HSW98 showing the phase positions of all M models of HSW98, TLW03 and this paper. Its counterpart for the P models is plotted in ISW04. Note that the outer layers of the model as seen in the central panel do not show the same periodicity as the central star, and that by examining only two full successive cycles we can include much of the cycle-to-cycle variation that one might observe using a longer time series (this is also clear in the P series plot in ISW04). Figure 2 shows a much longer time series of luminosity for both the P and M series models, showing the positions of the model series examined in this paper. It is clear from this plot that the M series has significantly less cycle-to-cycle variation than the P series. It is a general feature of extant red giant pulsation models that reducing the envelope mass increases the irregularity of the pulsation. The increased irregularity at lower total mass is probably related to the increasingly chaotic behaviour of the outer layers as the envelope mass is decreased (Icke, Franck and Heske 1992). Here, the M model envelope mass (about $0.6 M_{\odot}$) is 50 percent higher than that of the P series ($0.4 M_{\odot}$). Note that the cycles selected for detailed investigation in this paper are not particularly unusual.

The full set of M models is given in Table 1. In addition to the standard $\tau_{\text{Ross}}=1$ Rosseland radius R and the corresponding effective temperature $T_{\text{eff}} \propto (L/R^2)^{1/4}$, Table 1 also gives the $R_{1.04}$ filter radius, defined after Scholz & Takeda (1987) in a narrow $1.04 \mu\text{m}$ bandpass (centred at $1.0465 \mu\text{m}$, width $0.001 \mu\text{m}$, see JS02) and the corresponding effective temperature $T_{1.04} \propto (L/R_{1.04}^2)^{1/4}$. Since this bandpass shows very little contamination, $R_{1.04}$ is essentially the monochromatic $\tau_{1.04}=1$ optical-depth radius and describes the approximate position of the continuum-forming layers. Though this is a non-observable quantity, the ISW04 study shows that it is very close to an observable interferometric fit radius and probably is an excellent indicator of geometric pulsation of an M-type Mira variable. Note that the position of the $\tau_{\text{Ross}}=1$ layer is not well suited for describing geometric pulsation owing to the properties of the Rosseland mean of extinction coefficients (see e.g. HSW98; Scholz 2003; ISW04).

For both the P and the M model series, the transition region between the dust-free stellar atmosphere and the dust-driven stellar wind region is a significant cause of modelling uncertainty. These model series do not include dust formation. They have an arbitrary radius cutoff of $5 R_p$, and a minimum temperature of 740 K is adopted in the outermost layers where the state equation of gas particles is assumed to become unrealistic. Dust could form from about 2 to 3 continuum radii (e.g. Danchi et al. 1994; Danchi & Bester 1995; Habing 1996; Lobel et al. 2000; Lorenz-Martins & Pompeia 2000). It would influence the density stratification of the outer part of the atmosphere due to radiation pressure as well as the

Table 1. Parameters of M series Mira models. The model names ending in ‘n’ are the new models presented in this paper. The columns: visual phase ϕ_{vis} ; luminosity L ; Rosseland radius R ; $1.04 \mu\text{m}$ near-continuum radius $R_{1.04}$; effective temperatures T_{eff} and $T_{1.04}$ corresponding to R and $R_{1.04}$; reference for previously published models.

Mod.	ϕ_{vis}	L (L_{\odot})	R (R_p)	$R_{1.04}$ (R_p)	T_{eff} (K)	$T_{1.04}$ (K)	Ref.
M05	0+0.49	1470	0.93	0.84	2310	2420	HSW98
M06n	0+0.60	2430	0.78	0.78	2860	2860	
M08	0+0.77	4780	0.81	0.81	3320	3320	TLW03
M09n	0+0.89	5060	1.03	1.03	2970	2970	
M10	1+0.02	4910	1.19	1.18	2750	2760	HSW98
M11n	1+0.11	4360	1.26	1.21	2590	2640	
M12n	1+0.21	3470	1.30	1.18	2410	2540	
M12	1+0.27	2990	1.33	1.12	2300	2500	TLW03
M14n	1+0.40	1670	1.17	0.91	2110	2400	
M15	1+0.48	1720	0.88	0.83	2460	2530	HSW98
M16n	1+0.60	2460	0.77	0.77	2860	2860	
M18	1+0.75	4840	0.81	0.81	3310	3310	TLW03
M18n	1+0.84	4980	0.99	1.00	3020	3010	
M19n	1+0.90	5070	1.08	1.09	2900	2900	
M20	2+0.05	4550	1.23	1.20	2650	2680	HSW98
M21n	2+0.10	4120	1.26	1.21	2550	2610	
M22	2+0.25	2850	1.27	1.10	2330	2490	TLW03
M23n	2+0.30	2350	1.25	1.03	2230	2460	
M24n	2+0.40	1540	1.09	0.87	2160	2410	
M25n	2+0.50	2250	0.80	0.79	2770	2780	

temperature stratification due to radiation transport effects in case of noticeable thermodynamic coupling of dust and gas particles (cf. Bedding et al. 2001). In the dust-free M models, the temperature of about 1200 K where silicate grains may be formed is reached around 2 continuum radii (e.g. defined as $R_{1.04}$) at most phases and at about 3 continuum radii at pre-maximum phases of our 2nd cycle. In the dust-free P models, the 1200 K distance is more phase- and cycle-dependent and ranges from around 2 to more than 4 continuum radii. Corundum condensation occurs at about 1400 K but may be insignificant in M-type atmospheres (e.g. Gail & Sedlmayr 1998; cf. also Patzer 2004). Note, however, that dust temperatures in a dusty atmosphere tend to be higher at a given distance from the star’s centre than gas temperatures in a dust-free atmosphere, with details depending upon thermodynamic coupling between dust and gas (Bedding et al. 2001, e.g. their Figures 1 and 2 showing the models P20 and M10). Therefore, comparisons between the model series in this paper will focus on the wavelength regimes that are relatively insensitive to these outer atmospheric layers (i.e. where there is a relatively small optical depth at 2 to 3 continuum radii).

3 LIGHT CURVES

The model-predicted light curves in the K (simple rectangular bandpass, centred at $2.195 \mu\text{m}$, width $0.4 \mu\text{m}$, see JS02) and J ($1.25, 0.3$) bandpasses may be compared with the observations of *o* Cet and R Leo by Whitelock et al. (2000) which cover a large number of pulsation cycles and show clearly significant cycle-to-cycle variations. Figure 3 is a fit of model-predicted light curves covering two successive cycles of the P series (from model P10 at phase 1.00 to P30 at 2.98, Table 1 of ISW04) as well as the M series (from M05 at 0.49 to M25 at 2.50, Table 1) to the observations.

The fit includes a phase zero-point shift as well as a magnitude zero-point shift in the K bandpass (other filters are then fixed by this

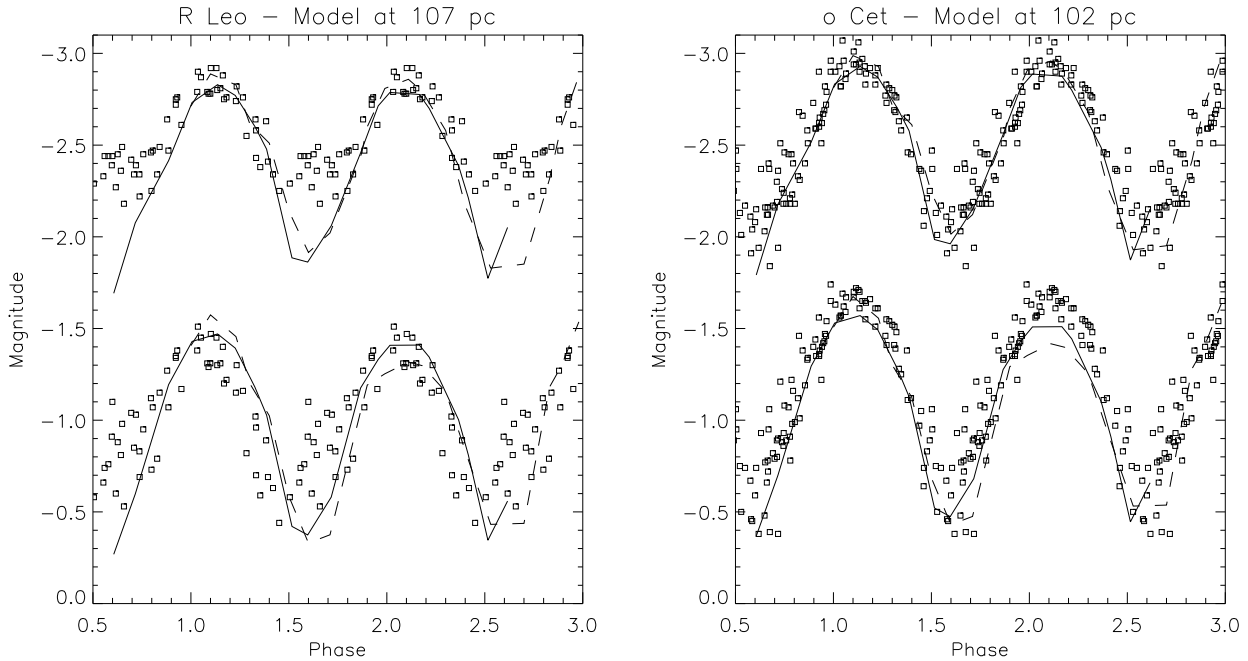


Figure 3. Light curves for the P (dashed line) and M (solid line) model series (K-band - upper plot, J-band - lower plot) with observations of Whitelock et al. (2000) overplotted. See text for phase adjustment of M series.

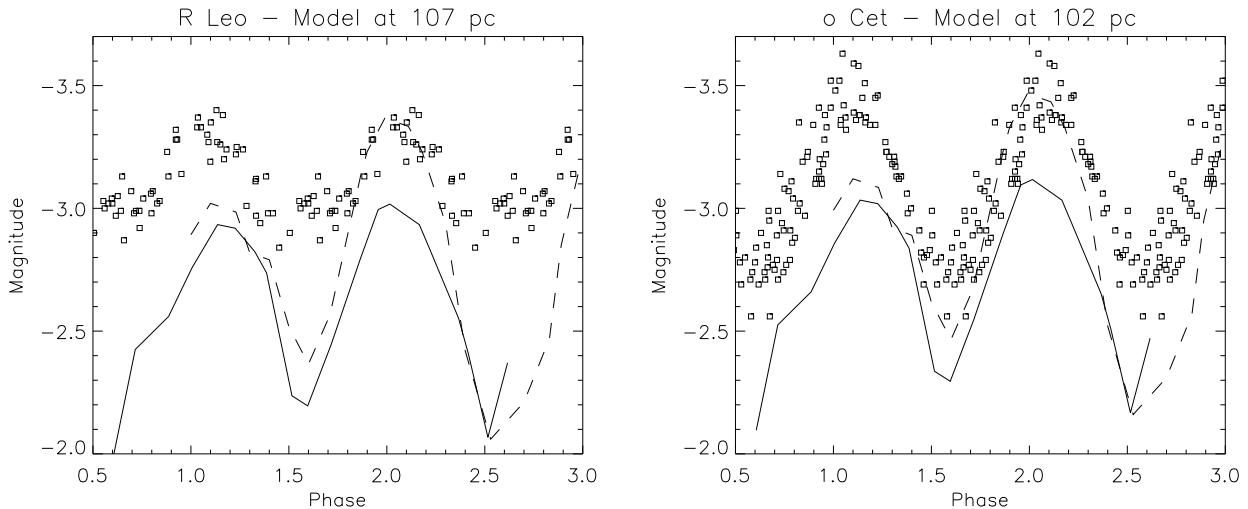


Figure 4. Light curves for the P (dashed line) and M (solid line) model series for the L band (see text) with observations of Whitelock et al. (2000) overplotted.

zero point) so that good agreement occurs near maximum. The visual minus K-band phase shift of M-type Miras is just marginally larger than the visual minus bolometric phase shift of 0.1 adopted in model phase assignment (difference less than 0.05, Smith et al. 2002). The difference between the K-fit phase shifts of our two model series (0.116) will be used throughout this paper for comparing the phase dependence of model-predicted quantities, i.e. +0.116 is added to M model phases of Table 1 in Figure 2 and all forthcoming figures. The model stars of both series would have to be placed at distances of 107 pc and 102 pc for emitting the near-maximum K magnitudes quoted by Whitelock et al. (2000) for the stars *o* Cet and R Leo respectively (ISW04, see the discussion given there as for HIPPARCOS distances). Note also that the periods of *o* Cet

(334 days) and R Leo (313 days) given by Whitelock et al. (2000) differ slightly from the model periods discussed in Section 2 (linear pulsation period of parent star: 332 days; period of P series: 341 days; period of M series: 317 days).

The agreement between model-predicted and observed light curves (Figure 3) is good, though neither star is perfectly modelled by the P or the M series and some significant differences are quite obvious, in particular the smaller amplitude of R Leo in the K bandpass. In fact, an excellent fit by the M model curve may be achieved for *o* Cet in both the K and J bandpasses if the M model star were placed at a slightly smaller distance, i.e. if the M curve were slightly shifted upwards in the figure. No comparably good fit by the P model curve is possible because of the much larger dif-

ference between the two cycles. The small K-band amplitude of R Leo is not predicted by either model series. Note that differences between our simple rectangular bandpass profiles and those used in the observations of Whitelock et al. (2000) account for only very small effects (see ISW04). We did not attempt to fit optical light curves as these are much less reliably predicted by the models owing to excessive temperature sensitivity in the Wien part of Planck functions and to the uncertainties of treatment of very strong TiO bands (cf. TLSW03).

Figure 4 shows the model light curves for the non-rectangular L bandpass as defined in Bessell and Brett (1988) with observations of Whitelock et al. (2000) overplotted. The cycle-to-cycle variations of the P series are clearly much more pronounced than either the M series or the observations. Furthermore, both model series (with the exception of the second maximum of the P series) have systematically lower fluxes than either star. This discrepancy is not surprising, because this bandpass (about $3.2\text{--}3.75\ \mu\text{m}$) is noticeably affected by relatively strong H_2O absorption in the outer layers of the model star (e.g. Tej, Lançon & Scholz 2003a), where there are significant modelling uncertainties (see Section 2). In contrast, bandpasses that are conventionally used as near-continuum bandpasses in interferometric work (e.g. Mennesson et al. 2002, L' 3.4-4.1; JS02, L* 3.5-4.1) avoid the strong- H_2O regime at the short- λ end of the L filter and are not so extremely sensitive to the structure of the outer atmosphere. Thus, reliable information about mass effects may be predicted by presently available models only from bandpasses with relatively little contamination from the outermost low-temperature layers of the star. It should be noted in this context that studies based upon empirical H_2O shells that may reproduce contamination effects in near-continuum bandpasses quite satisfactorily (e.g. Mennesson et al. 2002; Ohnaka 2004; Weiner 2004) are unable to predict the time and parameter dependent behavior of molecular absorption in a real Mira star.

We have also made a close comparison between the model photometry of the P and M series in near-continuum bandpasses, in order to search for mass indicators based on colour. We find that the cycle-to-cycle variation masks any possible systematic differences in colours between the two series, despite the fact that the M models are systematically cooler than the P models at near-maximum phases (cf. Table 1 with the table of ISW04).

4 INTERFEROMETRIC DIAMETERS

In this section, the behaviour of simulated high angular resolution imaging data products based on the P and M model series is investigated. Although, in the general case, the full model center-to-limb variation (CLV) will be required to interpret the output of a high resolution measurement, here we choose a simple but instructive metric. A uniform disk (UD) profile has been fitted to the computed model visibility function at a single spatial frequency where the visibility is first less than 0.3. In the case where the CLV strongly resembles a UD, it doesn't matter where the fit is made, and in the case where the CLV departs from a UD, the fit at 0.3 gives a fairly robust estimator of overall "size" without strong influence from the exact form of the profile. For complicated CLVs, different fitting profiles and spatial frequency ranges will yield varying results (see ISW04 for a discussion of this relating to the P series).

Figure 5 shows single-point UD radii from fits to the M model series. The cycle-to-cycle variation seen here is much less than in the P series as shown in the equivalent figure of ISW04 (Figure 5 in that paper). The bandpass differing most between the two series ap-

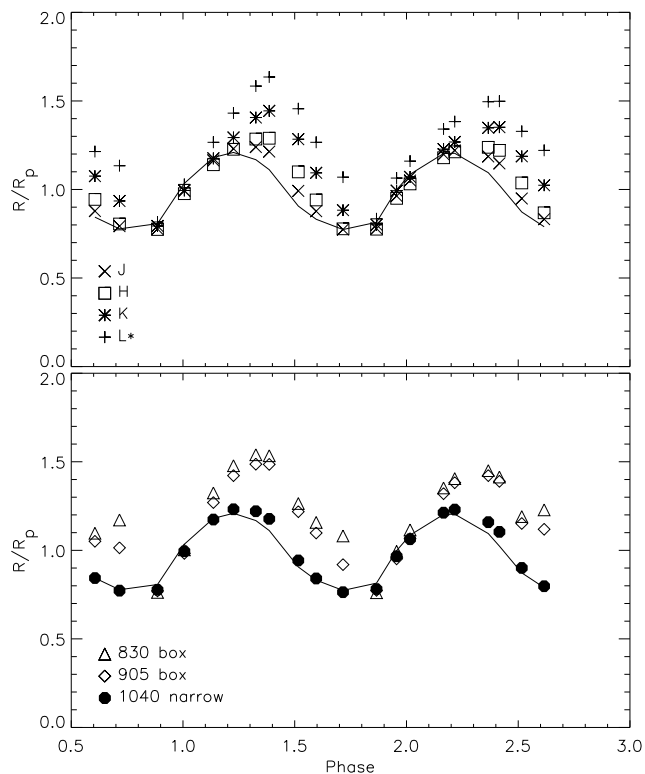


Figure 5. Radii from single-point $V=0.3$ uniform disk fits to the M model series in 7 near-continuum bandpasses (see text). The overplotted solid line in both panels is the $\tau=1$ optical-depth radii for the $1.04\ \mu\text{m}$ continuum bandpass ($R_{1.04}$).

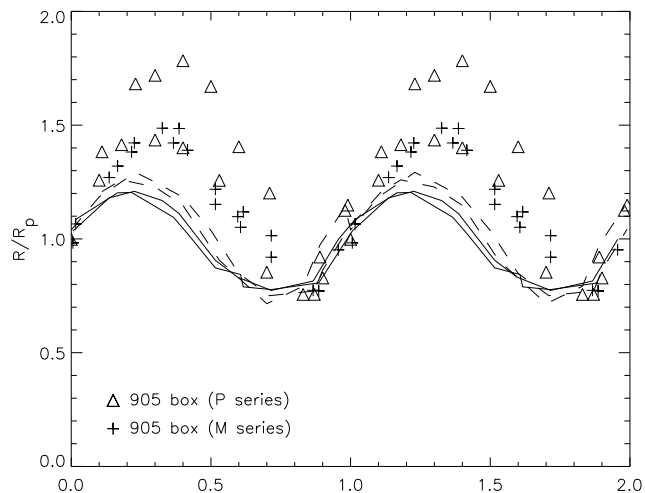


Figure 6. Radii from single-point $V=0.3$ uniform disk fits to both the P and M model series in the 905 nm bandpass, which is moderately contaminated by the TiO molecule. The $R_{1.04}$ radii (see text) are overplotted for the M (solid line) and P (dashed line) series. Both cycles of both series are folded-in to a single cycle and repeated so that comparison of any systematic differences between the models can be made.

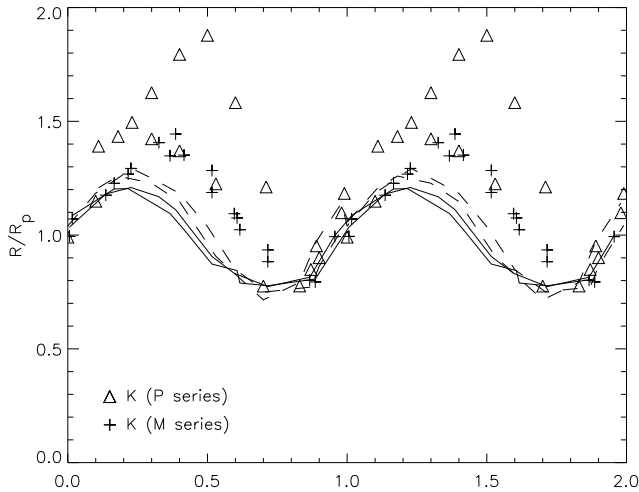


Figure 7. Radii of single-point $V=0.3$ uniform disk fits as in Figure 6 for the K bandpass, which is moderately contaminated by the H_2O molecule.

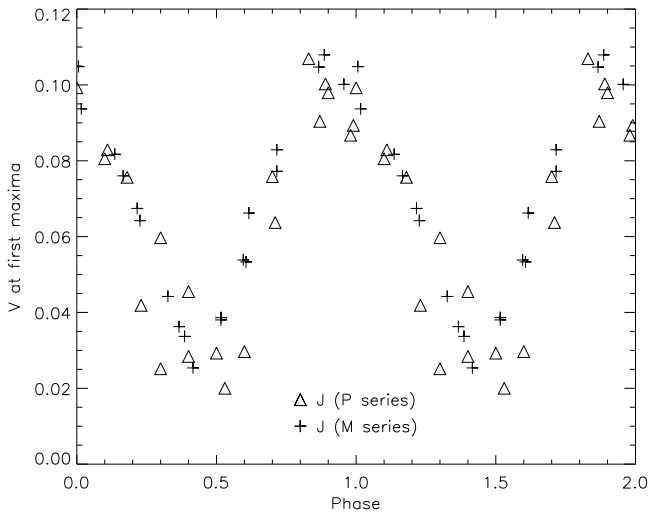


Figure 8. Height of the first maxima in the visibility curve for the J band for both the P and M series, which is a measure of the limb-darkening in this bandpass.

pears to be the L^* bandpass (centred on $3.799 \mu\text{m}$, width $0.6 \mu\text{m}$) which has much smaller apparent radii in the M series than in the P series. Note, however, that though this near-continuum bandpass avoids the strong- H_2O regime at the short-wavelength end of the conventional L bandpass, it is still substantially affected by fairly strong water absorption partly originating in relatively high atmospheric layers which have significant modelling uncertainties (see Section 2).

In order to make a closer comparison of key bandpasses, we show fit radii for both model series for both cycles folded in together in Figures 6 (905 nm bandpass, centred at $0.905 \mu\text{m}$, width $0.05 \mu\text{m}$) and 7 (K bandpass). These bandpasses were chosen as they are moderately contaminated by the important molecules TiO and H_2O , but are not sensitive to the low-temperature high layers in the models. For a more detailed discussion of molecular contamination including CLVs and optical depth radii, see JS02. It is clear

that the extreme cycle of the P series shows significantly larger apparent radii than either cycle of the M series, but if one were to pick a cycle at random, there is no systematic difference in these observables between the two model series. These figures also display the $\tau_{1.04}=1$ optical-depth radii $R_{1.04}$ in the narrow $1.04 \mu\text{m}$ continuum bandpass for the two series, which shows a variation of radius with phase that is only modestly different between the two series. First, we see that the $R_{1.04}$ pulsation amplitude is about 20 percent smaller for the more massive M series. However even in near-continuum bandpasses, this difference in $R_{1.04}$ is partly masked by small amounts of molecular contamination in interferometric diameter measurements.

It is important to note also that the parent-star radius R_p used for normalization in the figures is 8 percent larger for the M models. If two stars have the same core mass and, hence, the same luminosity but have different envelope mass, simultaneous measurements of the diameter in a weak-contamination bandpass and of multi-bandpass fluxes (for deriving the bolometric flux), should reveal a systematic difference in the effective temperature defined (e.g. $T_{1.04}$) in terms of the diameter in that bandpass. The higher-mass star is systematically cooler, and differences are phase-dependent (see $T_{1.04}$ entries in Table 1 of ISW04 and of this paper). Investigation of both the amplitude effect and the temperature effect requires high-precision interferometry and successive observations in a close phase sequence, covering a considerable phase interval and possibly several cycles, and has to be done as a differential comparison between two or more stars. A promising way to accomplish this would be closely-spaced (\sim weekly) near-continuum interferometry with simultaneous photometry catching pre-maximum phases of maximal compression and almost UD-like intensity distribution. A robust and precise measurement here should yield a maximum effective temperature which is little affected by upper-atmosphere molecular contamination and is systematically higher in the lower-mass P models than in the M models (see Table 1 in this paper and in ISW04).

The standard bandpass that shows minimum contamination by any molecule is the J bandpass. Although the values for the fit radius are very similar between the two series and are close to $R_{1.04}$, one might expect the different density profiles of the two model series to produce different shapes of their visibility curves. A means to test this hypothesis is to measure the height of the first maxima in the curve of visibility modulus versus baseline, which gives an estimate of limb-darkening. These values are plotted for both cycles of both series in Figure 8. This measurement would be 0.13 for a uniform disk, and 0.0 for a Gaussian CLV. It is clear that there is no systematic difference between the two series in this observable, implying similar brightness profiles.

As with the lightcurve analysis in the previous section, the strongest discriminant in the simulated observables from the P and the M model series appears to be the cycle-to-cycle variation. The lower-mass P models are certainly seen to produce more erratic behavior. It is debatable whether the present models can be trusted to the point of delivering a quantitative mass diagnostic based on these observed effects (see Section 2). However, differential studies of different stars may shed some light on relative differences in mass.

5 DISCUSSION

Changes of the structure of deeper atmospheric layers (in which the continuum is formed and in which the contamination of standard

near-continuum bandpasses is generated) are very modest when the envelope mass of the Mira is increased by a factor of 1.5 from 0.4 to 0.6 M_{\odot} . The resulting light curves and disk brightness distributions in these bandpasses are very similar for the here investigated P (envelope 0.4 M_{\odot}) and M (0.6) model series. A more significant mass dependence of the CLV one might suspect from the studies of HSW98 and JS02, is feigned by the strong phase dependence of the CLV shape. This phase dependence can only be recognized on the basis of a closely sampled time sequence. In fact, considering the fundamental uncertainties in phase assignment, sound interpretation of an interferometric diameter measurement at an isolated single phase may be extremely difficult. Significant mass effects *do* occur in the outer atmospheric layers which, however, are not readily accessible to model analysis owing to serious problems of modelling these layers.

The most conspicuous difference between the 1 M_{\odot} P series and the 1.2 M_{\odot} M series is the pronounced cycle-to-cycle variation of the P model series that is not found in the M series. Though quantitative details may be questioned in the present stage of modelling (Section 2), it is obvious from, for instance, light curves (e.g. Whitelock et al. 2000), TiO+VO colour index observations (e.g. Spinrad & Wing 1969), radial-velocity measurements (e.g. Joy 1954) and a few measurements of time-dependent diameters (e.g. Tuthill et al. 1995; Burns et al. 1998; Thompson et al. 2002) that noticeable cycle-to-cycle variations exist in Mira variables. From the light curves shown in Figures 3 and 5 (where the modelled curves in the L bandpass have to be considered with great caution, see Section 3), we suspect that the differences between the here selected two rather “extreme” cycles of the P series are larger than the cycle-to-cycle differences found in *o* Cet whereas the M series appears closer to a real star. Note that the two prototype Miras *o* Cet and R Leo that have very similar periods and spectral types (*o* Cet M5e-M9e, R Leo M6e-M9.5e, Whitelock et al. 2000) and are not known to show obvious spectral anomalies, have very different light curves in the K and L bandpasses. The amplitudes of R Leo are conspicuously small in K and L and cannot be predicted by any presently available model. We cannot exclude but seriously doubt that more pronounced mass variations would lead to a better model representation of R Leo.

For given period and luminosity, metallicity is the second fundamental parameter of a Mira variable besides mass. Metallicity is known to influence observable properties significantly (cf. Scholz & Wood 2004) and effects of changing the chemical composition are under investigation, but no quantitative results are available yet. Another source of differences between seemingly similar Miras are patchy structures of the atmosphere and other deviations from spherical symmetry, which have been observed in numerous stars including *o* Cet and R Leo (see the literature listed in Scholz 2003) but are outside the scope of the present spherical models. The conspicuous decrease of R Leo’s amplitude (compared to *o* Cet and the models) with increasing wavelength (J, K, L) could be due to either an effect of metallicity or non-spherical symmetry, or possibly a modest difference in luminosity between the two stars within the period-luminosity relationship scatter. It might also indicate the importance of a high- to circumstellar-layer phenomenon like, e.g., dust absorption that may depend sensitively upon the stellar mass (or metallicity) but is not properly described by our simple models. Note, however, that the simple models of Schuller et al. (2004) predict that dust optical-depths in both absorption and scattering are too small in R Leo to cause significant effects in these bandpasses.

6 CONCLUSIONS

An extensive study contrasting the observable properties of M-type Mira variables based on models of significantly different mass (1 M_{\odot} and 1.2 M_{\odot} or envelope masses of 0.4 M_{\odot} and 0.6 M_{\odot}) has been undertaken. No unequivocal signatures discriminating between these was found within the parameter space explored, covering observations of the lightcurves, CLV or apparent size behavior in selected filter bandpasses over the pulsation cycle. Three observational strategies, reliant on more precise and/or extensive measurement, showed promise in distinguishing high from low mass stars¹. The first of these would entail close observation covering a number of pulsation cycles, with the lower mass objects exhibiting greater cycle-to-cycle variations of spectrophotometric and interferometric properties. Other possible approaches are to search for small differences in the pulsation amplitude or in effective temperatures through careful and relatively precise measurement of apparent diameter in an (almost) uncontaminated bandpass.

ACKNOWLEDGMENTS

This research was supported by the Australian Research Council and the Deutsche Forschungsgemeinschaft within the linkage project “Red Giants”.

REFERENCES

- Bedding T.R., Jacob A.P., Scholz M., Wood P.R. 2001, MNRAS 325, 1487
 Bessell M.S., Brett J.M. 1988, PASP 100,1134
 Burns D. et al. 1998, MNRAS 297, 462
 Danchi W.C., Bester M. 1995, Ap&SS 224, 339
 Danchi W.C., Bester M., Degiacomi C.G., Greenhill L.J., Townes C.H. 1994, AJ 107, 1469
 Feast M.W., Glass I.S., Whitelock P.A., Catchpole R.M. 1989, MNRAS 241, 375
 Gail H.-P., Sedlmayr E. 1998, Faraday Discuss. 109, 303
 Habing, H.J. 1996, A&ARv, 7, 97
 Hofmann K.-H., Scholz M., Wood P.R. 1998, A&A 339, 846 (HSW98)
 Hughes S.M.G., Wood P.R. 1990, AJ 99, 784
 Icke V., Frank A., Heske A. 1992, A&A, 258, 341
 Ireland M.J., Scholz M., Wood P.R. 2004, MNRAS 352, 318 (ISW04)
 Jacob A.P., Scholz M. 2002, MNRAS 336, 1377 (JS02)
 Joy A.H. 1954, ApJS 1, 39
 Knapp G.R., Pourbaix D., Platais I., Jorissen A. 2003, A&A 403, 993
 Lobel A., Bagnulo S., Doyle J.G., Power C. 2000, MNRAS 317, 391
 Lockwood G.W., Wing R.F. 1971, ApJ 169, 63
 Lorenz-Martins S., Pompeia L. 2000, MNRAS 315, 856
 Mennesson B. et al. 2002, ApJ 579, 446
 Ohnaka, K. 2004, A&A, In Press
 Patzer A.B.C. 2004, in: Astrophysics of Dust, A.N. Witt, C. Clayton, B.T. Draine (eds), Astron. Soc. Pac. Conf. Ser., San Francisco, Vol. 309, 301
 Perrin G., Coudé du Foresto V., Ridgway S.T., Mennesson B., Ruilier C., Mariotti J.-M., Traub W.A., Lacasse M.G. 1999, A&A 345, 221
 Scholz M. 2003, in: Astronomical Telescopes and Instrumentation 2002, Interferometry for Optical Astronomy II, W.A. Traub (ed.), Proceedings SPIE, Bellingham, Vol. 4838, p.163
 Scholz M., Takeda Y. 1987, A&A 186, 200 (erratum: 196, 342)
 Scholz M., Wood P.R. 2004, in: IAU Coll. 193, Variable Stars in the Local Group, D.W. Kurtz, K. Pollard (eds), Astron. Soc. Pac. Conf. Ser., San Francisco, Vol. 310, p.313

¹ Predictions of existing and additional models are available upon request to anyone interested for specific observational programs.

- Schuller P. et al. 2004, A&A 418, 151
Smith B.J., Leisawitz D., Castelaz M.W., Luttermoser D. 2002, AJ 123, 948
Spinrad H., Wing R.F. 1969, ARA&A 7, 249
Tej A., Lançon A., Scholz M. 2003a, A&A 401, 347
Tej A., Lançon A., Scholz M., Wood P.R. 2003b, A&A 412, 481 (TL5W03)
Thompson R.R., Creech-Eakman M.J., Van Belle G.T. 2002, ApJ 577, 447
Tuthill P.G., Haniff C.A., Baldwin J.E. 1995, MNRAS 277, 1541
Weiner, J. 2004, ApJL, 611, L37
Whitelock P., Marang F., Feast M. 2000, MNRAS 319, 728
Woodruff H.C. et al. 2004, A&A 421, 703
Young J.S. et al. 2000, MNRAS 318, 381